MODELING OF TRANSCUTANEOUS ENERGY TRANSFER SYSTEM FOR AN IMPLANTABLE GASTROINTESTINAL STIMULATION DEVICE

Joanna Liu C. Wu, Damian I. Kachlakev, Martin P. Mintchev

Abstract: This study models a transcutaneous energy transmission system which can supply DC power to an implanted device without an external battery. The goals of the study are to: (1) develop a model to describe the transcutaneous energy transmission system; and (2) use the developed model to design a transcutaneous energy transmission system for an implantable gastrointestinal neurostimulator. The complete trancutaneous energy system includes a power amplifier, a highly inductive coupling structure, and an ac-to-dc rectifying circuit in the receiver. Power amplification is based on the single-ended class E amplifier concept. The power amplification stage is self-oscillating, and the oscillation frequency is influenced by the coupling of the coils. The highly inductive coupling structure employs the stage tuning concept. Design methods and detailed analysis are provided. The proposed model is verified through the implementation of the design.

1. Introduction

1.1. Gastrointestinal Stimulation

In the recent years, more and more scientific groups are interested in applying functional electrical stimulation to restore impaired motility in the gastrointestinal tract [1-11]. There are four distinct methods for GI electrical stimulation. The first method is to entrain slow wave activity in both animals [4] and humans [3] by "pacing" the organ at a frequency slightly higher than the intrinsic slow wave frequency, and approach similar to cardiac pacing. The second method applies current stimulation at 4-40 times the intrinsic slow wave frequency and has been reported to have some antiemetic effect. The most recent stimulation technique is known as neural gastrointestinal electrical stimulation (NGES) [12, 13]. This approach involves voltage stimulation at 50 Hz delivered through matched pairs of electrodes implanted in the smooth muscle of the stomach wall. The effect of this approach has been shown by accelerated microprocessor-controlled gastric emptying of both solids [10] and liquids [11] in the stomach, as well as by increased colonic transit in both acute and chronic canine models.

The success in the implementation of an NGES system is intimately and directly related to the development of a fully implantable but externally controllable multichannel device. Powering such implanted device becomes a principle challenge. There are four widely accepted techniques for powering an implanted device: (1) Conventional wire cord (focusing on the biocompatibility of the shielding materials), (2) stand-alone implantable battery, (3) radio frequency (RF, transcutaneous inductive) link technologies, and (4) a combination of (2) and (3) using implantable stand-alone rechargeable batteries.

1.2. Aim of the Present Study

The purpose of this feasibility study is to design a transcutaneous power transfer system for a neurostimulator design aiming at restoring impaired gastrointestinal motility. The first mention of powering an implanted device through a transcutaneous inductive coupling link was in 1934 [5]. The practical attempts appeared in the late 1970s [13]. There are two distinct paradigms for designing such a system. One paradigm is known as a loosely coupled link [14] which has a low degree of coupling between the transmitting and the receiving coils, while the other one is highly coupled inductive link, which has a relatively high degree of coupling between the coils. The highly coupled inductive link assumes transmitting and receiving coils of approximately the same size [15] and is the design aim of this project.

2. Methods

In the present study, the design of a highly coupled inductive link was considered.

2.1. Design Requirements

The voltage to be delivered to the implanted device would be in the range of 10 to 20 V DC for implanted stimulator current drawing between 0 and 50 mA [22]. The minimum and maximum equivalent loads are 200 Ω and 100 kΩ respectively [20]. The design requirements are presented in Table 1.

Design Requirement	Value
Minimum load voltage, V_{load}	10 V
Maximum load current, I_{load}	50 mA
Minimum value of load, $R_{loadmin}$	200 Ω
Maximum value of load, $R_{loadmax}$	100 kΩ
Power delivered to R_{load}	500 mW

Table 1:   Highly coupled inductive link design requirement

2.2. Design Procedure

The design procedure of a stagger-tuned inductive link is outlined in [15] and is briefly described below.

It has been demonstrated already that the minimum variation of gain of the inductive link occurs at 1.6 MHz. In the following procedure, it is assumed that the inductive link operates at an operating frequency of f_o = 1.6 MHz and the DC supply of the link is 9V.

2.2.1. Spiral Coil Design

In this project, the transmitter and receiver coils are both spiral coils and approximately of the same size. The methods used in calculating the self-inductance of such coils and the mutual inductance between the two coils have been previously reported [23, 13]. The calculation of the self-inductance of the spiral coils is based on the assumption that the spiral coils can be modeled as coaxial circular loops of wire.

I.   Calculation of the self-inductance of a spiral coil

The self-inductance of a single loop of wire can be calculated by:

$$L(a,w) = \mu_0 a \left(\ln\left(\frac{8a}{w}\right) - 2 \right) \tag{1}$$

where a is the radius of the single loop, w is the radius of the wire, and μ_0 is the magnetic permeability of the free space.

The mutual inductance of two spiral coils whose axes are parallel can be presented by:

$$M(a,b,\rho,d) = \mu o \sqrt{ab} \left[\left(\frac{2}{k} - k\right) K(k) - \frac{2}{k} E(k) \right] \tag{2}$$

where $k \equiv \left(\frac{4ab}{(a+b)^2 + d^2} \right)^{\frac{1}{2}}$

and where a and b are the radii of the two loops, d is the distance between the two loops, ρ is the axial misalignment, and K and E are the complete elliptic integrals of the first and second kind, respectively.

The self-inductance of such a coil is approximately equal to the summation of self-inductances of single loops, and with wire-radius w, the overall self-inductance is represented by:

$$L_a = \sum_{i=1}^{N_a} L(a_i, w) + \sum_{i=1}^{N_z} \sum_{j=1}^{N_a} M(a_i, a_j, \rho = 0, d = 0)(1 - \delta_{i,j}) \tag{3}$$

where $\delta_{i,j} = 1$ for $i = j$, and $\delta_{i,j} = 0$ otherwise.

II. Calculation of mutual inductance between two spiral coils

The mutual inductance between primary and secondary coils can be calculated by:

$$M_{ab} = \sum_{i=1}^{N_z} \sum_{j=1}^{N_a} M(a_i, b_j, \rho, d) \tag{4}$$

However, Eq. (4) is valid for the case with axial misalignment only. To calculate the exact mutual inductance between two coils with simultaneous axial and angular misalignments, an approximation is provided as:

$$M(a, b, \rho, d, \alpha) = \frac{M(a, b, \rho, d)}{\sqrt{\cos \alpha}} \tag{5}$$

where α is the angular misalignment. Once the calculation method of self-inductance of a spiral coil and mutual inductance of two spiral coils is introduced, the parameters of transmitter and receiver coil orientations need to be determined. The constraints of the design are listed in Table 2.

Coil Separation	0.5 cm - 2.0 cm
Axial Misalignment	0 cm - ±1.0 cm
Angular Misalignment	0° - 20°
Diameter of transmitter and receiver coil	5 cm

Table 2: Highly coupled inductive link coupling constraints

Matlab code was developed for calculating the self-inductances and the mutual inductance of the transmitter (L_t) and the receiver (L_r) coils, based on the outlined constraints. The maximum and minimum coupling coefficients, k_{max} and k_{min}, are then calculated according to Eq. (6) and (7), respectively.

$$k_{max} = \frac{M_{max}}{\sqrt{L_t L_r}} \tag{6}$$

$$k_{min} = \frac{M_{min}}{\sqrt{L_t L_r}} \tag{7}$$

Furthermore, in order to determine the optimal number of turns, the Matlab Design Tool was used to vary the number of turns in the transmitter and receiver coils, and to compare the performance of the resulting links. Increasing the number of turns in the two coils reduced the variation in the load voltage, and enhanced the overall efficiency of the link. For this design, 10-turn spiral coils were chosen for the transmitter (n_t) and the receiver (n_r). When the space between concentric turns of the coils was approximately 1.18 mm, the geometry of these coils resulted in a self-inductance $L_t, L_r = 4.07$ μH, with coupling coefficients $k_{min} = 0.26$ and $k_{max} = 0.82$.

2.2.2. Choosing the Operating Frequency f_o

In order to minimize the amount of magnetic field absorbed by the abdominal tissue, the frequency should be chosen to be as low as possible, since the absorption increases exponentially with frequency [25]. However, the power transfer capability of the inductive link improves with increasing operating frequency. In addition, it has

been already demonstrated that at a frequency of approximately 1.60 MHz, the variation in the gain is minimized [15]. Therefore, the frequency of f_o = 1.6 MHz was chosen as an operating frequency of the link.

2.2.3. Choosing the Resonant Frequency of the Receiver, f_r

The resonant frequency of the receiver was chosen such that $f_r / f_o > 1$. The trade off is that as f_r / f_o increases, the overall voltage output gain increases. In other words, if the overall gain is too small, the ratio of f_r / f_o should be moved away from unity. However, if the ratio of f_r / f_o increases, the overall gain variation also increases. To determine the optimal ratio of f_r / f_o, Matlab Design Tool was used to vary f_r / f_o and to compare the performance of the resulting links. Figure 1 shows different performances of the links with different ratios of f_r / f_o. After examining the magnitude and the variation of the load voltage for a set of values of f_r / f_o, it became apparent that for f_r / f_o = 1.2, the load voltage variation was minimized. This means the resonant frequency of the receiver was f_r = 1.92 MHz. The value of the shunt capacitor C_r can be calculated as follows:
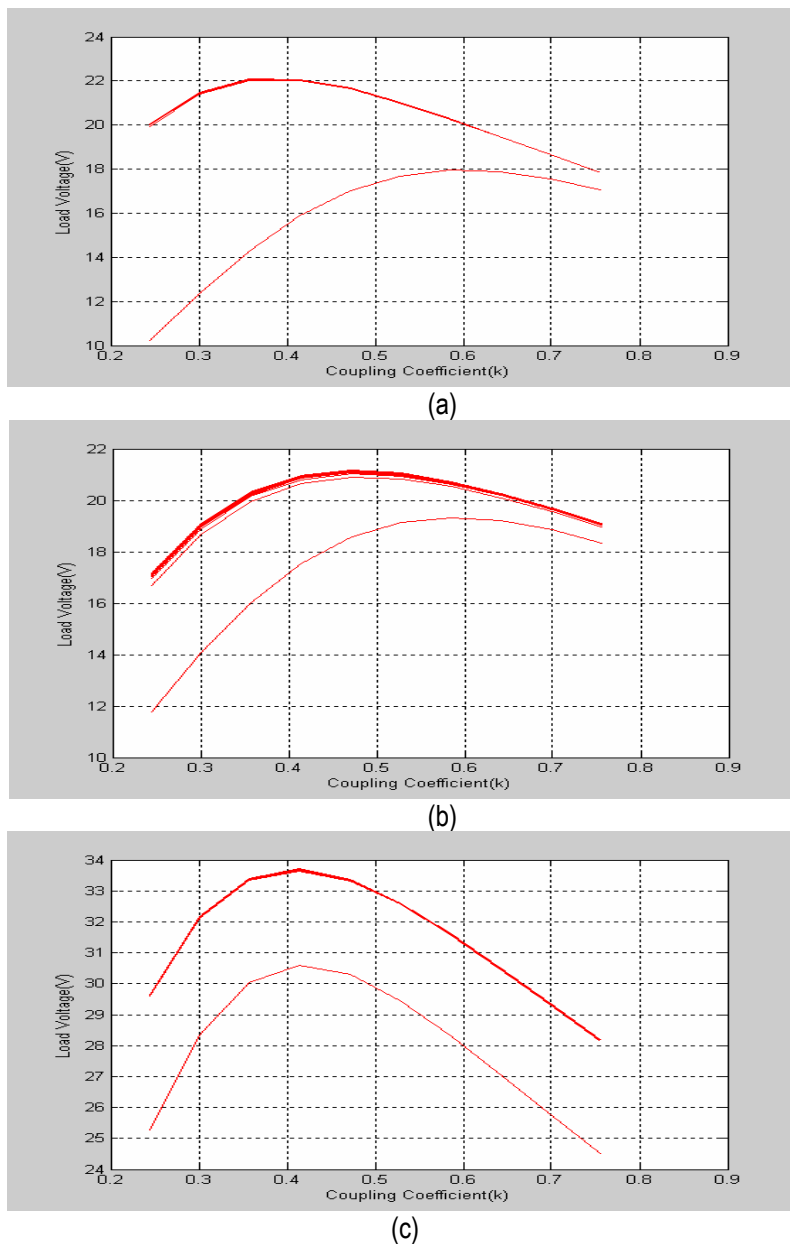
$$c_r = \frac{1}{\omega^2 L_r} \tag{8}$$

(a)

(b)

(c)

Figure 1: Load voltage over entire design space. (a) fr / fo = 1.1. (b) fr / fo = 1.2. (c) fr / fo = 1.4.

2.2.4. Choosing Resonant Frequency of Transmitter, f_t

Next, the resonant frequency of transmitter, f_t, is calculated by Eq. (9) [11].

$$\omega_t = \sqrt{\frac{\left(\omega^2\right)\left(1 - H + \dfrac{1}{Q_t^2}\right)}{1 + \sqrt{H - \dfrac{1}{Q_T^2}}}} \qquad (9)$$

In which

$$H = \frac{k_{opt}^4\left[\left(\dfrac{\omega^2}{\omega_r^2}\right)^2 + \dfrac{1}{Q_r^2}\right]}{\left(1 - \dfrac{\omega^2}{\omega_r^2}\right) + \dfrac{1}{Q_r^2}} \qquad (10)$$

$$k_{opt} = \sqrt{k_{min}k_{max}} \qquad (11)$$

$$Q_t = \frac{\omega L_t}{R_t}, \quad Q_r = \frac{R_r}{\omega L_r} \qquad (12)$$

With the determined tuning ratio, f_r / f_o, the receiver resonant frequency was determined with Eq. (2.5.13), and the transmitter resonant frequency was calculated as f_t = 1.12 MHz. The tuning capacitor of the transmitter is

$$c_t = \frac{1}{\omega^2 L_t} \qquad (13)$$

Finally, Matlab Design Tool was used to determine the maximum and the minimum DC load voltages from the highly inductive link in order to specify the tolerance for the voltage regulation and other components for the rest of the transcutaneous energy transfer system. The plot of the maximum and the minimum load voltages for the inductive link is presented in Figure 2.
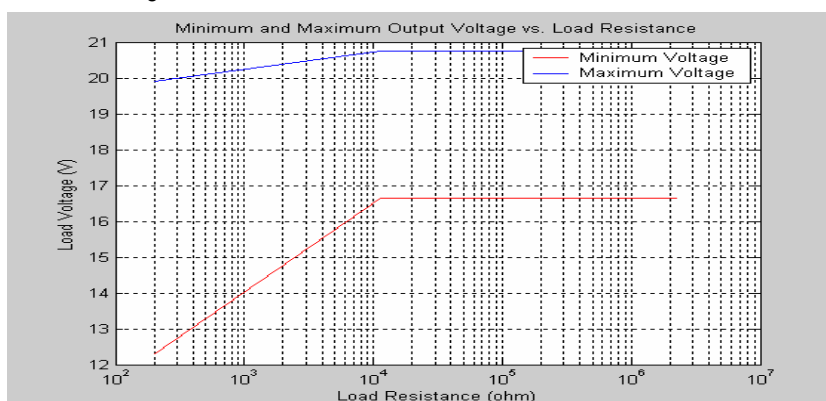

Figure 2:   The maximum and minimum load voltage for the highly coupled inductive link.

3. Results

3.1. Spiral Coil Characterization

In order to reduce the power losses in the transmission load, Litz wire was used to make the spiral coils. Both the transmitter and the receiver coils were constructed using 270/46, 22 Gauge equivalent Litz wire (New England

Electric Wire Corp., Lisbon, NH, USA). The number of turns in both coils was 10, and space between concentric turns of the coils was approximately 1.18 mm. There are two methods employed to validate the coil models, as described in Section 2.5.2.1. The first method is to use an LCR meter to extract the self-inductance and the equivalent series resistance (ESR) values from the coils. The values extracted from RLC meter for frequencies of 120 Hz, 1 KHz, and 10 KHz are presented in Tables 3, 4, and 5 respectively.

	Measured Self-inductance (µH)	Calculated Self-inductance (µH)	Percent Difference (%)	ESR (mΩ)
Transmitter coil	4.0	4.07	1.72	170
Receiver coil	4.05	4.07	0.49	170

Table 3: Self-inductance and ESR values extracted from RLC meter in 120 Hz

	Measured Self-inductance (µH)	Calculated Self-inductance (µH)	Percent Difference (%)	ESR (mΩ)
Transmitter coil	3.58	4.07	12.01	168
Receiver coil	3.77	4.07	7.37	168

Table 4: Self-inductance and ESR values extracted from RLC meter in 1 kHz

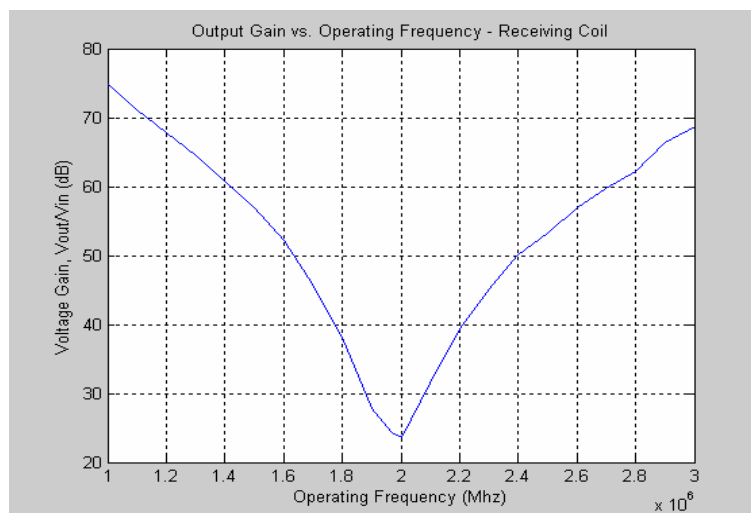|	Measured Self-inductance (µH)	Calculated Self-inductance (µH)	Percent Difference (%)	ESR (mΩ)
Transmitter coil	3.53	4.07	13.26	168
Receiver coil	3.71	4.07	8.85	168

Table 5: Self-inductance and ESR values extracted from RLC meter in 10 kHz

Measured values of self-inductance at a low frequency (120 Hz in this case) agreed with the calculated values, while the percent difference between measured and calculated values increased with the increment of the operating frequency. This means that the self-inductance value of a spiral coil changes when the operating frequency changes. Alternatively, a testing circuit was implemented to extract these same values. In the circuit, R was 10 Ohm and C was 1.78 nF. An *HP 33120A* function generator was used to drive the circuit. An *Agilent 54621D* oscilloscope measured the output voltage of the coils V_{out}. If the resistance of the circuit was small, the resonant frequency occurred at $\omega L = \dfrac{1}{\omega C}$. Also, the resonant frequency occurred when the impedance reaches maximum. The frequencies used for characterizing the circuit varied from 100 Hz to 3 MHz. Matlab Design Tool was used to plot the output voltages of the coil at various frequencies (Figure 3).

Observing Figure 3, the resonant frequencies of the transmitter and the receiver coils were 1.9 MHz and 2.0 MHz, respectively. According to $L = \dfrac{1}{(2\pi f)^2 C}$, the self-inductance of the transmitter and the receiver coils can be calculated.
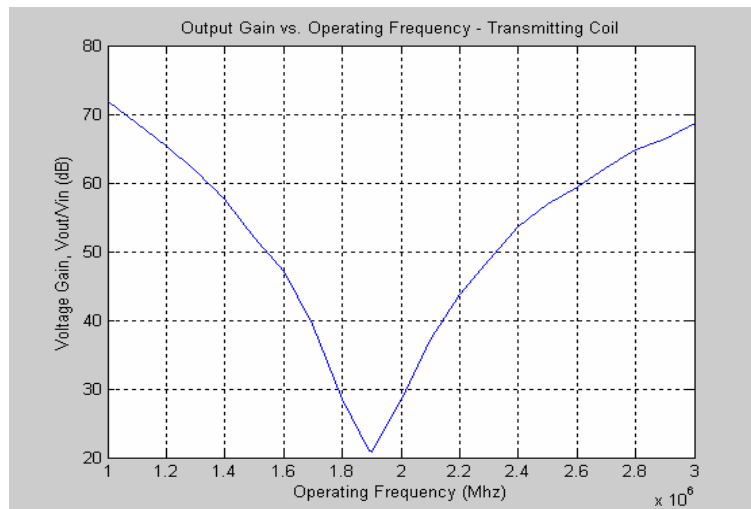
(a)

(b)

Figure3: Frequency response of spiral coils. (a) transmitter coil; and (b) receiver coils.

The values of the self-inductance of the coils are shown in Table 6.

	Measured Self-inductance from resonant circuit (μH)	Calculated Self-inductance (μH)	Percent Difference (%)
Transmitter coil	3.52	4.07	13.5
Receiver coil	3.50	4.07	14.0

Table 6: Self-inductance values extracted from parallel resonant circuit

Comparison between the data from Tables 3, 4, and 5 shows that there is a gap greater than 10% between the measured and calculated values when frequency is higher than 1 kHz. The values in Table 6 were extracted from the frequency response of the resonant circuit. The circuit was built on a breadboard. The breadboard might affect the performance of the circuit. As a result, the difference between measured and calculated values in the above tables is reasonable, since the value of calculated inductance is frequency independent and the measured values of the self-inductance decrease with increasing the operating frequency. To obtain a more accurate result at the operating frequency of 1.6 MHz, a network analyzer is recommended.

3.2. Implementing the Highly Coupled Inductive Link

The implementation of the highly coupled inductive link is based on the coils characterized in the previous section. First, the implementation of the transmitter begins with the calculation of the component values of class E power amplifier according to the methodology described in Section 2.4. The values of the choke inductor, the parallel capacitor, and the series capacitor are listed in Table 7 below.

Component name	Value
Chock inductor, L_{chock}	33 µH
Parallel capacitor, C_p	12 nF
Series capacitor, C_t	3.3 nF

Table 7: Calculated values of the components in the transmitter

Second, the shunt capacitor and the filter capacitor in the receiver need to be determined. The value of the filter capacitor C_f can be calculated according to the voltage rise time required by the stimulator unit described in [21]. The values of both components, C_r and C_f, are presented in Table 8.

Component name	Value
Filter capacitor, C_f	15 nF
Shunt capacitor, C_t	1.2 nF

Table 8: Calculated values of component in the receiver

3.3. Highly Coupled Inductive Link Testing

The measurement of the DC output voltage with various load resistances was based on a coil separation of 1.8 cm with an axial misalignment of 0° and an angular misalignment of 0°. The values of the resistive load varied from 100 Ω to 3.3 kΩ. The measured and calculated results are present on Figure 4.
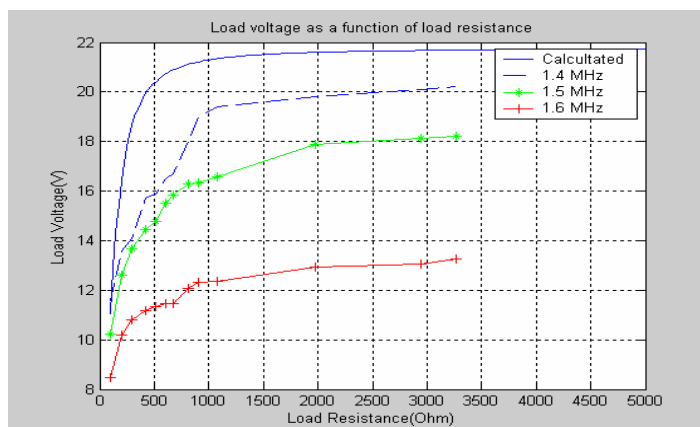

Figure 4: Measured and calculated values of the highly transcutaneous inductive link
with various load resistances.

Figure 4 depicts the difference between the measured maximum and minimum load voltages, which is minimized when the operating frequency is 1.6 MHz. However, the difference between the calculated (ideal case) and measured load voltages is maximized at the same frequency. It is observed that the maximum variation between the measured maximum and minimum load voltages occurs at 1.4 MHz. To optimize the transcutaneous inductive link, 1.5 MHz is chosen as the operating frequency for the link, instead of 1.6 MHz,.

3.4. Power Transfer Efficiency

One may be interested in the overall power transfer efficiency η of a highly coupled transcutaneous inductive link. Under a typical coupling condition, with a coil separation of 15 mm, and 5 mm of axial misalignment, the overall DC power from the transmitter was delivered to a DC load ranging from 100Ω to 3200Ω,as presented in Figure 5. The overall energy transfer efficiency of the transcutaneous energy transformer is presented in Figure 6.

Figure 5 reveals that the overall energy transfer efficiency is maximized at 33% when the DC load, R_{load}, is 100Ω. When R_{load} is 200Ω, the efficiency reaches 28%.
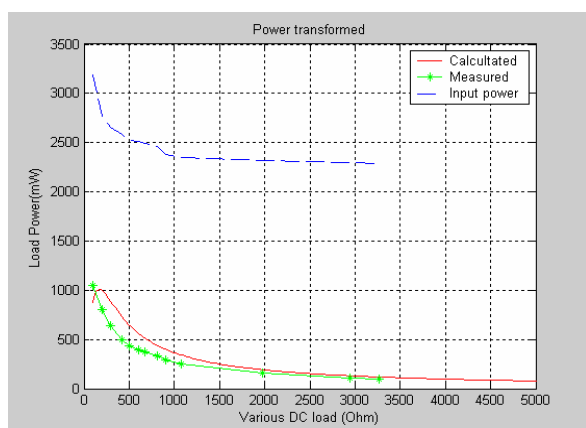
Figure 5: Input power from the transmitter, calculated and measured power to the implanted load
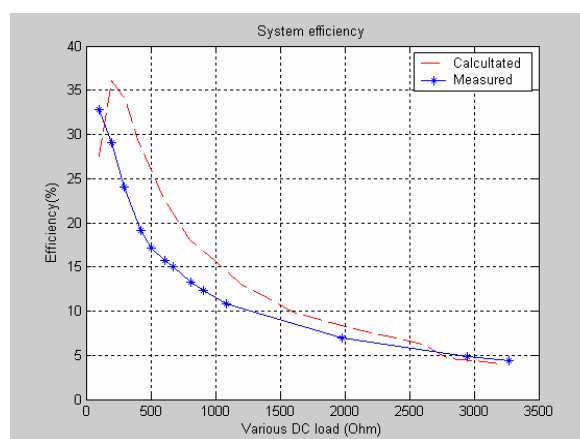
Figure 6: Overall power transfer efficiency of the highly transcutaneous inductive link.

Conclusion

In this study a comprehensive design and testing of a transcutaneous energy transfer system for an implanted system is provided, specifically targeted for gastrointestinal stimulation. The robust modeling of the transcutaneous transformer has been validated through the design, implementation, and testing stages. The measured results for the transformer are in a good agreement with the predicted values.

Bibliography

[1] J.E. Everhart (Ed). Digestive Diseases in the United States: Epidemiology and Impact. National Institutes of Health Publication No. 94-1447, 1994

[2] A. M. Bilgutay et al. Gastro-intestinal pacing: a new concept in the treatment of ileus. Annals of Surgery, 158(3), 139-144, 1963.

[3] J.D. Huizinga. Electrophysiology of human colon motility in health and disease. Clinics in Gastroenterology, 15(4), 879-901. 1986.

[4] S. Grundfest-Bronialowski et al. Electrical control of intestinal reservoirs in a chronic dog model. ASAIO Transactions, 34:664-668, 1988.

[5] E.L. Chaffee and R.E. Light. A method for remote control of eclectrical stimulation of the nervous system. Yale J. Biol. Med., 7, 1934.

[6] T. Cameron et al. Micro modular implants to provide electrical stimulation of paralyzed muscles and limbs. IEEE Trans. Biomed. Eng., 44(9):781-790, September 1987.

[7] K. Bruninga et al. The effect of electrical stimulation on colonic transit following spinal cord injury in cats. Spinal cord. 36:847-53, 1998.

[8] S. Grundfest-Broniakowski et al. voluntary control of and ideal pouch by coordinated electrical stimulation, a pilot study in the dog. Dis Colon Rectum. 31:261-7, 1998

[9] S.F. Hughes et al. electrically stimulated smooth muscle neosphincter. Br J Surg. 82:1321-61, 996.

[10] M. P. Mintchev et al. Microprocessor controlled movement of solid gastric content using sequential neural electrical stimulation. Gastroenterology, 118, 258-263. 2000.

[11] M. P. Mintchev et al. Microprocessor controlled movement of liquid gastric content using sequential neural electrical stimulation. Gut, 43, 607-611, 1998.

[12] M.P. Mintchev and K.L. Bowes. Computer model of gastric electrical stimulation. Ann. Biomed. Eng., 25:726-730, April 1997.

[13] W.H. Ko et al. Design of radio-frequency powered coils for implant instruments. Med. & Biol. Eng. & Comput., 15:634-640, 1977.

[14] N. de N. Donaldson and T.A. Perkins. Analysis of resonant coupled coils in the design of radio frequency transcutaneous links. Med. & Biol. Eng. & Comput., 21:612-627, 1983.

[15] D.C. Galbraith et al. A wide-band efficient inductive transdermal power and data linkwith coupling insensitive gain. IEEE Trans. Biomed. Eng., 34(4):265-275, April 1987.

[16] O. Soykan, Power sources for implantable medical devices, Device Technology & Application (ELECTRONICS). 2002.

[17] M. K. Kazimierzuk, D. Czarkowski. Resonant power converters. Wiley-Interscience Publication, 1995, ISBN 0-471-04706-6.

[18] Nathan O. et al. Class E – A new class of high-efficiency tuned single-ended switching power amplifiers. IEEE Journal of solid-state circuits, vol. SC-10, No. 3, June 1975

[19] F.H. Raab. Idealized operation of the class E tuned power amplifier. IEEE Trans. Cir. Sys., CAS-24(12):725-735, December 1977.

[20] J.A. Doherty et al. Trancutaneous powering of implantable micro-stimulators for functional restoration of impaired gastrointestinal motility. In proceeding of the 25th Annual International Conference of the IEEE EMBS of the IEEE Engineering in Medicine and Biology Society, Cancun, Mexico, 2003, pages 1575-1578, 2003.

[21] J. Doherty. Implantable, transcutaneously powered neurostimulator system to restore gastrointestinal motility. M.Sc. Thesis, University of Calgary, Calgary, Alberta, Canada, 2005.

[22] D. Onen. Implantable, transcutaneously powered neurostimulator system to restore gastrointestinal motility. M.Sc. Thesis, University of Calgary, Calgary, Alberta, Canada, 2005.

[23] C. M. Zierhofer, E. S. Hochmair. Geometric approach for coupling enhancement of magnetivally coupled coils. IEEE Trans. Biom. Eng., 43(7):708-714, July, 1996.

[25] T. Akin. An integrated telemetric mulit-channel sieve electrode for nerve regerneration applications. Ph.D. dissertation, University of Michiagan, Ann, Arbor, MI, USA, 1994

Authors' Information

Joanna Liu C. Wu – Undergraduate Student, Department of Electrical and Computer Engineering, University of Calgary, Calgary, Alberta, Canada T2N1N4;e-mail: joannawu@enel.ucalgary.ca

Major Fields of Scientific Research: Embedded Systems, Electronic Instrumentation

Damian I. Kachlakev – Professor, Department of Civil and Environmental Engineering, California Polytechnic State University, San Luis Obispo, California, USA, Member of the ACI, the ASCE, the ASTM, the International Association for Bridges and Structural Engineering, the International Society for Plastics in Construction, the Society of Plastics Industry, and the Composite Institute. E-mail: dkachlak@calpoly.edu

Major Fields of Scientific Research: Composite Materials

Martin P. Mintchev – Professor, Department of Electrical and Computer Engineering, University of Calgary, Calgary, Alberta, Canada T2N1N4; Fellow, American Institute for Medical and Biological Engineering, Washington, DC, USA; e-mail: mintchev@ucalgary.ca

Major Fields of Scientific Research: Biomedical Instrumentation, Navigation, Information Systems in Medicine